Title	Phospholipid Molecular Layer that Enhances Distinction of Odors Based on Artificial Sniffing
Author(s)	Yotsumoto, Mai; Matsuo, Muneyuki; Kitahata, Hiroyuki; Nakanishi, Shinobu; Denda, Mitsuhiro; Nagayama, Masaharu; Nakata, Satoshi
Citation	ACS Sensors , 8 (12) : 4494 - 4503
Issue Date	2023-12-07
DOI	
Self DOI	
URL	https://ir.lib.hiroshima-u.ac.jp/00056140
Right	This document is the Accepted Manuscript version of a Published Work that appeared in final form in ACS Sensors, copyright © American Chemical Society after peer review and technical editing by the publisher. To access the final edited and published work see https://doi.org/10.1021/acssensors.3c00382 This is not the published version. Please cite only the published version. この論文は出版社版ではありません。引用の際には出版社版をご確認、ご利用ください。
Relation	


Hiroshima University Institutional Repository

Phospholipid molecular layer that enhances distinction of odors based on artificial sniffing

Mai Yotsumoto,[a] Muneyuki Matsuo,[a] Hiroyuki Kitahata,[b] Shinobu Nakanishi,[c] Mitsuhiro Denda,[d] Masaharu Nagayama,[e] and Satoshi Nakata*[a]

a. *Graduate School of Integrated Sciences for Life, Hiroshima University, 1-3-1 Kagamiyama, Higashi-Hiroshima, Hiroshima 739-8526, Japan*

b. *Graduate School of Science, Chiba University, Yayoi-cho 1-33, Inage-ku, Chiba 263-8522, Japan*

c. *Shiseido Global Innovation Center, 1-2-11, Takashima-cho, Nishi-ku, Yokohama, Kanagawa 220-0011, Japan*

d. *Institute for Advanced Study of Mathematical Sciences, 8F High-Rise Wing, Nakano Campus, Meiji University, 4-21-1 Nakano, Nakano-ku, Tokyo, 164-8525, Japan*

e. *Research Institute for Electronic Science, Hokkaido University, N10 W8, Kita-Ward, Sapporo 060-0810, Japan*

KEYWORDS : sniffing, surface tension, phospholipid molecular layer, odor-sensing, dynamic response

ABSTRACT: We propose a novel odor-sensing system based on the dynamic response of phospholipid molecular layers for artificial olfaction. Organisms obtain information about their surroundings based on multi-dimensional information obtained from sniffing, i.e., periodic perturbations. Semiconductor- and receptor-based odor sensors have been used previously. However, these sensors predominantly identify odors based on one-dimensional information, which limits the type of odor molecule they can identify. Therefore, development of odor sensors that mimic the olfactory systems of living organisms is useful to overcome this limitation. In this study, we developed a novel odor-sensing system based on the dynamics of phospholipids that responds delicately to chemical substances at room temperature using multi-dimensional information obtained from periodic perturbations. Odor molecules are periodically supplied to the phospholipid molecular layer as an input sample. The waveform of the surface tension of the phospholipid molecular layer changes depending on the odor molecules and serves as an output. Such characteristic responses originating from the dynamics of odor molecules on the phospholipid molecular layer can be reproduced numerically. The phospholipid molecular layer amplified the information originating from the odor molecule, and the mechanism was evaluated using surface pressure-area isotherms. This paper offers a platform for an interface chemistry-based artificial sniffing system as an active sensor and a novel olfactory mechanism via physicochemical responses of the receptor-independent membranes of the organism.

Sensation is important for maintaining life. For example, harmful chemicals can be smelled out and avoided. Olfaction is one of the five senses that responds directly to chemical stimuli. Most studies on olfactory mechanisms have focused on receptors, and the number of olfactory receptors discovered was approximately 350. However, we could identify far more odors.[1, 2] The number of functional olfactory receptors that were discovered previously is insufficient to characterize odorant discrimination performance,[3] and the mechanism by which we can distinguish a variety of odors has not yet been understood. Lipids, which are components of cell membranes,[4-6] or inorganic membranes,[7] may be involved in chemical identification and molecular recognition. We previously reported that the surface pressure (Π) is characteristically changed by the addition of volatile compounds owing to their interactions with phospholipid molecules.[8] These results suggest that the response of a phospholipid membrane toward odor molecules can amplify its discrimination ability.

Organisms exhibit excellent odor detection. Chemical information, such as molecular structure and concentration, is converted into multi-dimensional information on the time-variation of the electrical signal; for example, the frequency, amplitude, and shape of oscillations, which are generated by the excitation of nerve cells via receptors.[9, 10] In olfaction, it is thought that the temporal response obtained by sniffing is used to obtain such multi-dimensional information.[11-18] We smell by periodically inhaling the outside air. This process is called sniffing, and the air currents generated by sniffing periodically transport odor molecules to the olfactory epithelium, enabling the acquisition of higher-dimensional information.[19] Sniffing also allows air to be breathed in and reset; the odor is concentrated, and the odor molecules are adsorbed in the olfactory epithelium. Sniffing is necessary to obtain information from odors, and organisms regulate the amount of information received by controlling their sense of smell according to the external environment.[20] Accordingly, exploiting the dynamic response of the sensory system to periodic perturbations is a key strategy for identifying odor molecules.

Previous odor sensors included semiconductor gas sensors,[21,22] receptor-type sensors[23-26] and their artificial neural networks, and sensor arrays.[27, 28] Most of these sensors identify odors based on instantaneous information, which limits the range of odor molecules that can be identified and requires steady states.[29] On the other hand, in a few sensors, dynamics of semiconductor gas sensors have been utilized to identify gases.[19, 21, 22, 30] Therefore, we focused on odor identification via an elastic sensor system comprising phospholipids; the system is sensitive to chemical substances at room temperature and is based on multi-dimensional information obtained from periodic perturbations.

In this study, we developed a novel odor evaluation system based on artificial sniffing, using phospholipid molecular layers as a material. An electric fan periodically applied a flow to supply an odor stimulus to the 1,2-dipalmitoyl-*sn*-glycero-3-phosphocholine (DPPC) molecular layer distributed on water. Linalool, acetic acid,

and triethylamine were selected as the odorants. The time variation of surface tension of the DPPC molecular layer changed characteristically for individual odors. In particular, the response of the DPPC molecular layer to triethylamine was markedly different from that to acetic acid or linalool. Surface pressure (Π)–area (A) isotherms of the DPPC molecular layer and thermograms of DPPC were obtained to evaluate the interactions between DPPC and the odor molecules. Such characteristic responses to odor molecules can be qualitatively reproduced by numerical calculations based on the dynamics of odor molecules and the surface tension of the phospholipid molecular layer, depending on the type of odorant molecule. These results suggest that the dynamic responses generated by periodic perturbations are effective in distinguishing odors.

EXPERIMENTAL SECTION

DPPC was purchased from Sigma-Aldrich (MO, USA). Racemic linalool and chloroform were purchased from Nacalai Tesque, Inc. (Kyoto, Japan). Acetic acid was purchased from Tokyo Chemical Industry Co. Ltd. (Tokyo, Japan). Triethylamine was purchased from FUJIFILM Wako Pure Chemical Corporation (Osaka, Japan). Water was purified by filtering through active carbon, an ion-exchange resin, and a Millipore Milli-Q filtering system (Merck Direct-Q 3UV, Germany; resistance: 18 MΩ cm). Figure 1 shows a schematic illustration of the experimental system used to detect the dynamic response of a DPPC molecular layer by means of "sniffing." Purified water (50 mL) was poured into a large glass petri dish (inner diameter: 95 mm) with a mesh wire (width: 1 mm) 7mm above as the water phase (water depth: 8 mm). To obtain the phospholipid molecular layer on water, a 0.5 mM DPPC chloroform solution (volume: ~30 μL) was gently added dropwise to the water and the chloroform was evaporated from the water surface by leaving for 5 min. As a result, 1.54×10^{-8} mol of DPPC was distributed on the water as a molecular layer. A square voltage waveform (peak-to-peak voltage: 0–4 V, frequency: 0.02 Hz, temporal ratio between On (4 V) and Off (0 V) fan voltage: 50%), generated using a waveform generator (1920A, NF Electronic Instruments, Yokohama, Japan), was supplied to the electric fan for the sniffing operation. A filter paper (WHATMAN, 5211-090, USA, diameter: 30 mm) soaked in an odor sample (acetic acid, linalool, or triethylamine, amount of substance: 1.55 mmol, volume: 89–275 μL) was fixed with a mesh wire 7 mm above the water surface. The surface tension at the air/aqueous interface was measured using a Surface Tensiometer (CBVP-A3, Kyowa Interface Science Co. Ltd., Saitama, Japan) based on the Wilhelmy method,[31] in which a platinum plate (length: 23 mm, thickness: 0.5 mm, height: 10 mm) was placed 38 mm away from the center of the petri dish. The distance between the fan and the water surface was set at 30 mm to reduce fluctuation of air/water interface due to the air blowing and to supply a large amount of odorant. On the other hand, the distance between the mesh wire and the water surface was set at 7 mm to prevent the mesh wire from touching the water surface and to evenly supply odorants into the Petri dish. The experiments were performed in an air-conditioned room at 298 ± 2 K. At least four examinations were performed under each experimental condition to confirm the reproducibility of the experimental results.

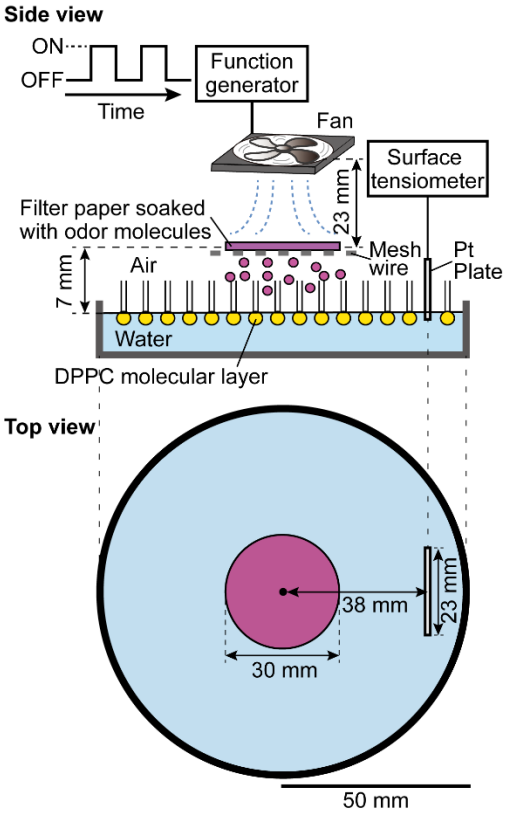

Figure 1. Experimental apparatus for detecting the dynamic response of a phospholipid molecular layer to an odor by means of 'sniffing'.

The flow rate was measured using a digital velocity meter (Testo 445, Testo GmbH & Co., Lenzkirch, Germany). Figure 2 shows the time variation of the input fan voltage (0.02 Hz) and obtained flow rate. The velocity meter sensor was placed in line with the filter paper. The flow rate was varied to converge to the maximum or minimum value under the application of a square-wave voltage to the fan.

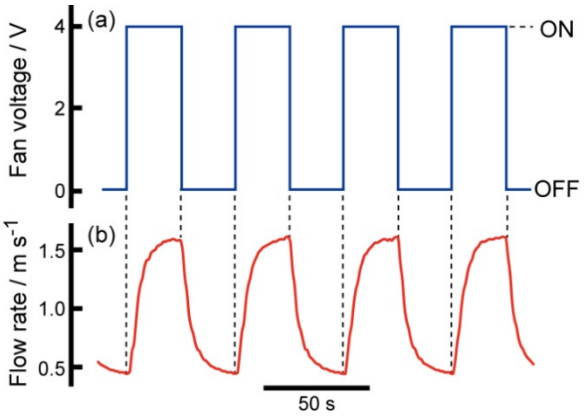

Figure 2. Time variation on (a) fan voltage and (b) flow rate. The frequency of the square wave voltage to operate the fan in (a) was 0.02 Hz. The data for (a) and (b) were measured simultaneously.

Π-A isotherms of the DPPC molecular layer were obtained using a surface pressure meter (Kyowa Interface Science Co. Ltd., HMB, Saitama, Japan) at 292 ± 1 K. A DPPC solution containing 1.62×10^{-8} mol DPPC was added dropwise onto the aqueous surface of a 4.0 mM triethylamine or acetic acid solution. The DPPC-

linalool mixed chloroform solution that was added dropwise onto the aqueous surface contained 1.62×10^{-8} mol of DPPC and linalool. The surface area (A) was reduced by a barrier from 210 to 21 cm^2 at a rate of 16.5 cm^2 min^{-1} (e.g., 17 $Å^2$ $molecule^{-1}$ min^{-1} for the DPPC molecular layer). Compression of the DPPC molecular layer was initiated 5 min after the addition of a chloroform solution containing DPPC to remove the solvent by evaporation. Four measurements, at minimum, were performed on each sample to confirm the reproducibility of the Π-A isotherm.

RESULTS

Dynamic responses of the surface tension and their fast Fourier transform (FFT) analysis. In this study, we used linalool, acetic acid, and triethylamine as the odor molecules. Figure 3 shows the experimental results obtained for the time-variation of the difference in surface tension $\Delta\gamma$ (= $\gamma - \gamma_{DPPC}$) under artificial sniffing, during which the sample odor molecules are periodically blown onto the DPPC molecular layer. In the figure, γ_{DPPC} and γ are the surface tensions of DPPC, without or with odors, respectively. The results obtained at the lower limit of A (= 100 $Å^2$ $molecule^{-1}$), where the surface tension is 2–3 mN m^{-1}, are shown in Figure S3.

To confirm the effect of the temperature of the aqueous phase, we examined the time-variation in γ by changing the temperature of the aqueous phase (Figure S5). The waveform of $\Delta\gamma$ changed characteristically depending on the odor type. Here, $\Delta\gamma$ was used to determine the characteristic responses of the odor molecules. That is, if $\Delta\gamma$ is zero, there is no change in the surface tension of the DPPC molecular layer upon the addition of odor molecules. $\Delta\gamma$ for linalool and acetic acid decreased and increased when the fan voltage was switched On and Off, respectively. The amplitude of $\Delta\gamma$ for linalool was larger than that for acetic acid. By contrast, the time-variation of $\Delta\gamma$ for triethylamine was inverted; that is, $\Delta\gamma$ increased and decreased when the fan voltage was switched On and Off, respectively. The slopes and directions of the γ *vs*. flow-rate curves for linalool and acetic acid were negative and clockwise, respectively. By contrast, the slope and direction of the γ *vs*. flow rate curve for triethylamine were positive and followed a figure of eight-shaped trajectory, respectively. Such a figure of eight-shaped trajectory for trimethylamine was also reproduced qualitatively under the same conditions. 40 and 310 s after the periodic stimulation of acetic acid and triethylamine, γ was reverted to that for DPPC only. In contrast, γ was maintained after the addition of linalool. The time variations of γ_{DPPC} and γ for linalool, acetic acid, and triethylamine and the flow rate *vs*. γ_{DPPC} or γ curves are shown in Figure S1.

The concentrations of linalool, acetic acid, and triethylamine calculated from the vapor pressures of the odor molecules are 2.11×10^2 ppm, 4.61×10^4 ppm, and 6.81×10^4 ppm, respectively.

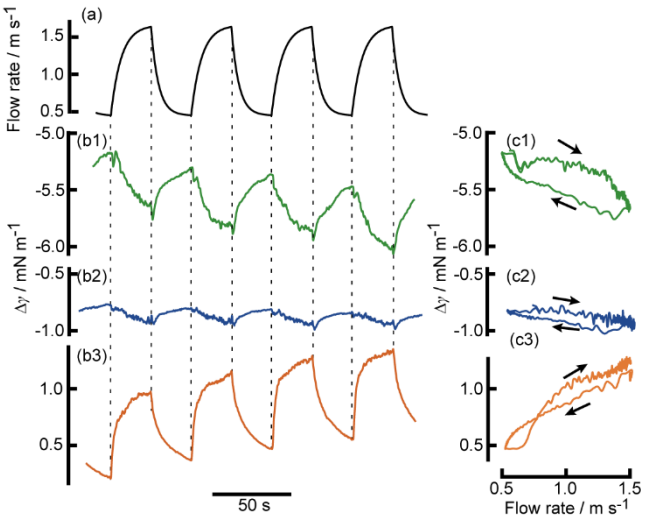

Figure 3. Time variation of (a) flow rate and (b) $\Delta\gamma$ under the application of periodic blowing air with odors ((1) linalool, (2) acetic acid, (3) triethylamine). (c) One cycle of $\Delta\gamma$ *vs*. flow rate of (b). The amounts of these odors soaked into a filter paper were 1.55 mmol. The data correspond to those for Figure S1.

The amount of triethylamine soaked in the filter paper was varied to confirm the quantitative response, $\Delta\gamma$. Figure 4 shows the time variation of $\Delta\gamma$ with the addition of different amounts of triethylamine under artificial sniffing. The amplitude of $\Delta\gamma$ increased; in other words, the positive slope of $\Delta\gamma$ *vs*. the flow rate increased with an increase in the amount of triethylamine. In addition, the degree of rapid and slow increases in $\Delta\gamma$ during the positive scan of the flow rate increased depending on the amount of triethylamine. The time variations of γ for triethylamine and the γ *vs*. flow rate curves with different amounts are shown in Figure S2.

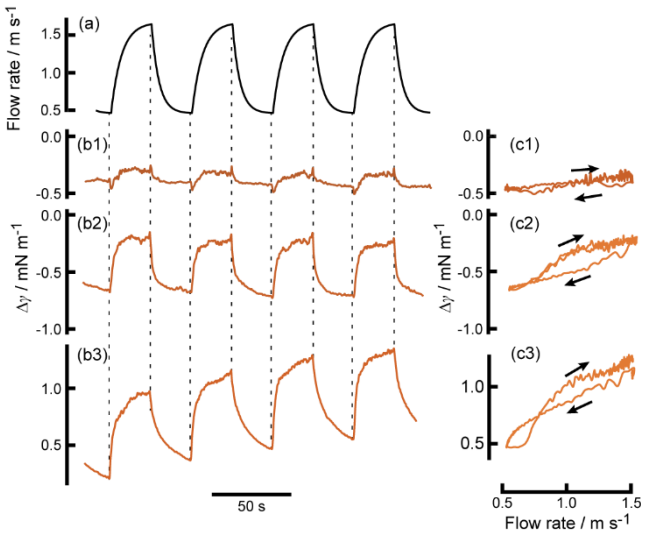

Figure 4. Time variation of (a) flow rate and (b) $\Delta\gamma$ under the application of periodic blowing air with triethylamine. (c) One cycle of $\Delta\gamma$ *vs*. flow rate of (b). The amounts of triethylamine soaked into a filter paper were (1) 0.31, (2) 0.78, and (3) 1.55 mmol. The data correspond to those for Figure S2.

To evaluate the characteristic responses to odor molecules, the time-variation of γ was Fourier transformed into the frequency domain (Figure 5).[19, 22, 32] The time variation of $\Delta\gamma$ was corrected to maintain a constant average value for the FFT procedure for triethylamine. The initial value for the FFT analysis was half that of

the total time during which the fan voltage was switched On. If $\Delta\gamma$ does not change with the addition of odor molecules, a graph that traces the dotted pentagon is obtained. R_n and I_n represent the real and imaginary parts of the nth harmonic, respectively, at a frequency of 0.02 Hz. If the slopes of $\Delta\gamma$ *vs*. flow rate curves are positive and negative, R_1 are positive and negative, respectively (Figures 3, 5, 8, and 10) since R_1 corresponds to the cosine function. On the other hand, if the rotational directions of $\Delta\gamma$ *vs*. $f(t)$ curves are clockwise and anticlockwise, I_1 are positive and negative, respectively (Figures 3, 5, 8, and 10) since I_1 corresponds to the sine function. R_1 corresponds to the slope of the flow rate *vs*. γ curve. R_1 underwent a negative change when linalool and acetic acid were added (Figures 5a and 5b for linalool and acetic acid, respectively) and a positive change when triethylamine was added (Figure 5e for triethylamine). The magnitude of these changes also increased with increasing triethylamine concentrations. I_1 for linalool and acetic acid underwent a positive change (Figures 5a and 5b), whereas that for triethylamine underwent a negative change (Figure 5e). I_2 and I_3 for triethylamine underwent a positive change (Figure 5e).

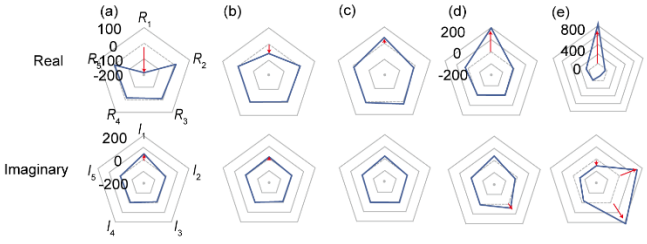

Figure 5. Amplitude of the fast Fourier transform (FFT, real part (R_n, n = 1, 2, 3, 4, and 5), and imaginary part (I_n, n = 1, 2, 3, 4, and 5)) for (a) 1.55 mmol linalool, (b) 1.55 mmol acetic acid, and (c) 0.31 mmol triethylamine, (d) 0.78 mmol triethylamine, and (e) 1.55 mmol triethylamine). Subscript, n = 1, 2, 3, 4, and 5, denotes the fundamental (0.02 Hz), 2nd (0.04 Hz), 3rd (0.06 Hz), 4th (0.08 Hz), and 5th harmonic (0.10 Hz) of FFT, respectively. The dotted pentagon denotes the amplitude of FFT for DPPC alone. The characteristic changes in the amplitudes were marked by the red arrows. The data correspond to those for Figures 3 and 4.

Surface tension at steady state. The surface tension of the DPPC molecular layer under equilibrium conditions, γ_e, was measured to clarify the dynamic response of γ to odor molecules under the application of artificial sniffing (Figure 6). γ_e decreased with increasing linalool or acetic acid concentrations. By contrast, γ_e increased with increasing triethylamine concentration. The slopes of the γ_e *vs*. C curves for linalool, acetic acid, and triethylamine are -3043, -884, and 398 N m^{-1} M^{-1}, respectively.

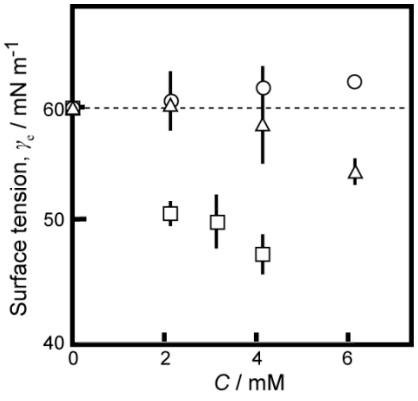

Figure 6. Surface tension under the equilibrium condition, γ_e, for the DPPC molecular layer depending on the concentration of linalool (squares), acetic acid (triangles), and triethylamine (circles) dissolved into the water phase under no flow. The surface tension was measured four times for each experimental condition. 1.54×10^{-8} mol DPPC was dropped on the water surface (surface area: 70.88 cm^2). Error bars indicate standard errors.

***Π–A* isotherm of the DPPC monolayer with the addition of odors.** The *Π–A* isotherms of the DPPC monolayer with the added linalool, acetic acid, and triethylamine were measured to clarify why triethylamine increased the surface tension of the molecular layer but linalool and acetic acid decreased it (Figure 7). In this experiment, 4 mM triethylamine or acetic acid aqueous solution was used as the water phase, and linalool chloroform solution (36 μL, 1.62 × 10^{-8} mol) was added dropwise onto the water phase and then evaporated to measure the *Π–A* isotherm for the mixture of DPPC and an odor molecule. At 70 < A < 90 Å^2 molecule^{-1}, Π of DPPC with the added acetic acid and linalool was higher than that without an odor molecule. By contrast, the Π of DPPC with the added triethylamine was lower than that of DPPC without an odor molecule.

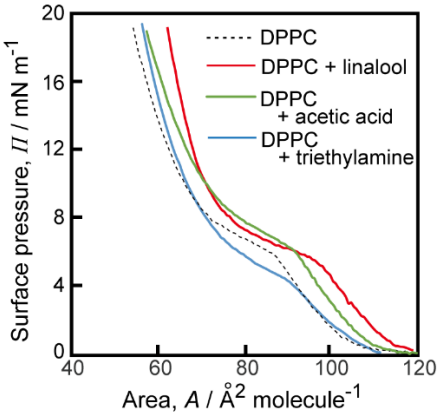

Figure 7. *Π-A* isotherms of DPPC monolayers without additives (dotted line), that with linalool (red line), that with acetic acid (green line), and that with triethylamine (blue line).

Numerical calculation and its FFT analysis. Next, we performed numerical calculations to clarify the mechanism underlying the characteristic responses of γ for DPPC to odor molecules. Here, we assumed that the dynamics of the DPPC molecular layer distributed on the water surface were ignored to simplify the numerical calculation. The dynamics of the odor molecules supplied to the water surface by periodic flow are described in eqs. 1 and 2:

$$du/dt = k_a w - (k_d + k_w)u, \quad (1)$$

$$dw/dt = f(t)w_0 - k_e w + k_d u, \quad (2)$$

where u (mol m^{-2}) is the surface concentration of the odor molecules adsorbed onto the water phase; w (mol m^{-2}) is the two-dimensional concentration of odor molecules in the subphase located near the water/air interface; k_a, k_d, k_w, and k_e (s^{-1}) are the rate constants for the adsorption of odor molecules from the subphase to the water phase, desorption of odor molecules from the water surface to the subphase, desorption from the water surface to the water phase, and movement from the surface to the bulk air phase, respectively; w_0 (mol m^{-3}) is the concentration of odor molecules in the bulk air phase; $f(t)$, as the flow rate (m s^{-1}), is the periodic function of the supplement of odor molecules using the electric fan.

$f(t)$ is expressed by eq. 3, which is based on the experimental results shown in Figure 2.

$$f(t) = \begin{cases} a_1 + b_1 exp[-c_1 t], & 0 \le t < T/2 \\ a_2 - b_2 exp[-c_2 t], & T/2 \le t < T \end{cases}, \quad (3)$$

where T(s) denotes the artificial sniffing period (49.6 s). One cycle of $f(t)$ is shown in Figure S7. $a_1 = 0.45$, $b_1 = 1.19$, $c_1 = 0.22$, $a_2 = 1.66$, $b_2 = 1.21$, and $c_2 = 0.16$. It should be noted that $f(0) = f(T)$, and $f(t)$ is continuous at $t = T/2$.

In the present calculation, the dynamics of the DPPC molecular layer were ignored to simplify the system and observe the dynamics of the odor molecules. $\Delta\gamma$ (mN m^{-1}) is expressed as in eq. 4.

$$\Delta\gamma = -\alpha u, \quad (4)$$

where α (N m^{-1} M^{-1}) is a constant that corresponds to the ratio of the slopes of the γ_e *vs.* C curves for the odorants in Figure 6.

Figure 8 shows the results obtained from the numerical calculations based on eqs. 1–4 to reproduce the characteristic change in $\Delta\gamma$ depending on the parameters. Actually, numerical results were obtained by dissolving the ordinary differential equations 1 and 2 with the Euler method (software: Microsoft Excel, the time resolution: 0.2 s). k_d and k_w were set based on the literature on the vapor pressure and water solubility, respectively, of the odor molecules used.[33-37] The time variations of $\Delta\gamma$ for linalool (Figure 3b1), acetic acid (Figure 3b2), and triethylamine (Figure 3b3) were qualitatively reproduced by those for Figures 8b1, b2, and b3, respectively. For example, at $df(t)/dt > 0$, $\Delta\gamma$ for (b1) and (b2) decreased, whereas that for (b3) increased. However, at $df(t)/dt < 0$, $\Delta\gamma$ for (b1) and (b2) increased, whereas that for (b3) decreased. The slopes of the $\Delta\gamma$ *vs.* flow rate curve and the directions of rotation for (c1) and (c2) were the same as those for linalool and acetic acid (Figures 1c1 and c2, respectively).

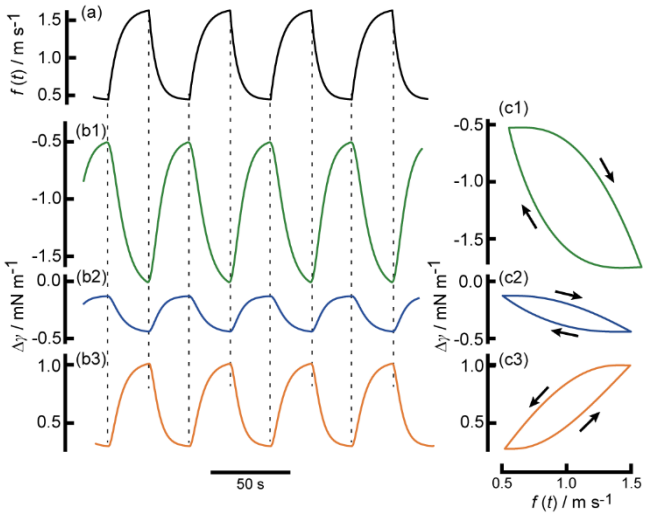

Figure 8. Results of the numerical calculation on the time-variation of (a) flow rate, $f(t)$ and (b) $\Delta\gamma$. (c) $\Delta\gamma$ *vs.* flow rate, $f(t)$. $w_0 = 0.1$ and k_a = (1) 0.08, (2) 0.2, and (3) 1.5. k_d = (1) 0.7, (2) 0.9, and (3) 0.6. k_w = (1) 0.1, (2) 0.8, and (3) 0.8. k_e = (1) 0.4, (2) 0.5, and (3) 1.5. α = (1) 37, (2) 9, and (3) -5.

Figure 9 shows the results of the numerical calculations based on eqs. 1–4; the results confirm the dynamic change in $\Delta\gamma$ which depends on the concentration of the odor molecules. $\Delta\gamma$ increased at $df(t)/dt > 0$ but decreased at $df(t)/dt < 0$. In addition, the slopes of the $\Delta\gamma$ *vs.* flow rate curves were positive. These results suggest that the experimental results were qualitatively reproduced by the numerical calculations.

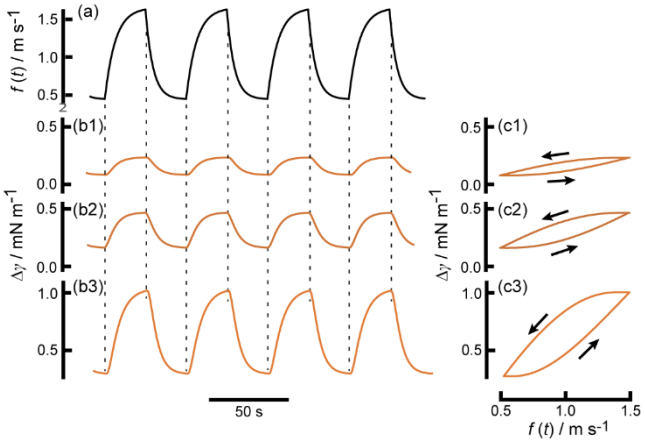

Figure 9. Results of numerical calculation on the time-variation of (a) flow rate, $f(t)$ and (b) $\Delta\gamma$. (c) $\Delta\gamma$ *vs.* flow rate, $f(t)$. $k_a = 1.5$, $k_d = 0.6$, $k_w = 0.8$, $k_e = 1.5$, and $\alpha = -5$. w_0 = (1) 0.02, (2) 0.05, and (3) 0.1.

The numerical results obtained for the time-variation of $\Delta\gamma$ (Figures 8b and 9b) were Fourier-transformed into the frequency domain (Figure 10). The fundamental and higher harmonics of the FFT changed characteristically depending on the parameters selected. We compared the experimental (Figure 5) and numerical (Figure 10) FFT results. For example, negative (linalool and acetic acid in Figures 5a and 5b) and positive (triethylamine in Figures 5c, 5d, and 5e) changes in R_1, which corresponded to the slope of the $\Delta\gamma$ *vs.* flow rate curve, were reproduced by numerical calculations (Figures 10a and 10b for negative changes, and Figures 10c, 10d, and 10e for positive changes). The positive (linalool and acetic acid in Figures 5a and 5c, respectively) and negative (triethylamine in Figure 5e) changes in I_1 were also reproduced by numerical calculations (Figures 10a and 10b for positive changes and Figure 10e for negative changes). The positive change in I_3 (Figure 5e for triethylamine) was reproduced by numerical calculations (Figure 10e).

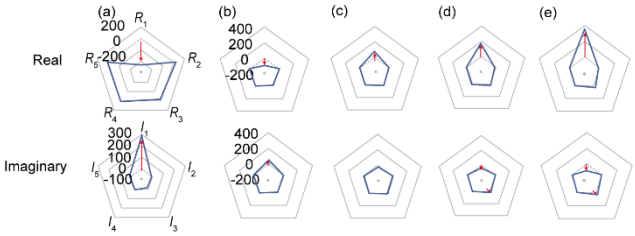

Figure 10. Amplitude of the fast Fourier transform (FFT, real part (R_n, n = 1, 2, 3, 4, and 5), imaginary part (I_n, n = 1, 2, 3, 4, and 5)) for numerical results in (a) Figure 8b1, (b) Figure 8b2, (c) Figure 9b1, (d) Figure 9b2, and (e) Figure 9b3. Subscript, n = 1, 2, 3, 4, and 5, denotes the fundamental (0.02 Hz), 2nd (0.04 Hz), 3rd (0.06 Hz), 4th (0.08 Hz), and 5th harmonic (0.10 Hz) of FFT, respectively. The dotted pentagon denotes the amplitude of FFT for DPPC alone. The characteristic changes in the amplitudes were marked by the red arrows.

DISCUSSION

We discuss the dynamic responses of the surface tension under the application of periodic perturbations, such as sniffing, based on the experimental results obtained herein and those of related studies.[1-32] In this study, we used linalool, acetic acid, and triethylamine as

the different types of odor molecules. That is, linalool is a hydrophobic compound, and acetic acid and triethylamine play the roles of acid and base, respectively.

Figures 3 and 4 suggest that the dynamic response of the DPPC molecular layer under periodic perturbation characteristically changes depending on the type of odor and systematically changes depending on the concentration of trimethylamine. As indicated in Figure S1, $\gamma_s = 60$ mN m^{-1} for DPPC without odorants corresponds to $\Pi = 72 - 60 = 12$ mN m^{-1}. A at 12 mN m^{-1} is 60 Å^2 molecule^{-1}, which corresponds to the close packing (Figure 7) since the cross-sectional area for a DPPC molecule is 57 Å^2. Noise of the surface tension during switch ON in Figures 3 and 4 is generated by the fluctuation of the platinum plate due to the air blowing to the air/water interface.

Figure 5 suggests that the characteristic responses of $\Delta\gamma$ to odor molecules can be qualitatively and quantitatively evaluated using the fundamental and higher harmonics of FFT spectra. Negative changes in R_1 and positive changes in I_1 (Figures 5a and 5b) correspond to the negative slope of the $\Delta\gamma$ *vs*. flow rate curve, as observed for linalool and acetic acid, and the clockwise rotation of the $\Delta\gamma$ *vs*. flow rate curve, respectively. By contrast, a positive change in R_1 and a negative change in I_1 correspond with the positive slope of the $\Delta\gamma$ *vs*. flow rate curve and the figure of eight-shaped rotation of the $\Delta\gamma$ *vs*. flow rate curve for triethylamine, respectively. The positive change in I_2 (see Figure 5c, 5d and 5e) suggests that the adsorption and desorption dynamics of triethylamine on the DPPC molecular layer differ between On- and Off-fan voltage operations. If higher harmonics with even number orders, such as R_2, I_2, R_4, and I_4, are observed, the On and Off processes are asymmetric. The characteristic changes in R_3 and I_3 (see Figure 5c, 5d and 5e) are due to the dynamics of adsorption/desorption as a nonlinear response.[22]

Figure 6 suggests that the change in γ_e, which depends on the concentration of odor molecules, induces the slope of the $\Delta\gamma$ *vs*. flow rate curve. That is, because γ_e for linalool and acetic acid decrease with an increase in their concentrations, the slopes of the $\Delta\gamma$ *vs*. flow rate curves are negative. Since γ_e for triethylamine increases with increasing concentration, the slope of the $\Delta\gamma$ *vs*. flow rate curve becomes positive.

Figure 7 suggests that the odor molecules enhance the phase transition of the DPPC monolayer from the LE phase to the LE + LC phase, rather than water alone.[38] Similarly, differential scanning calorimetry thermograms suggest that triethylamine affects the phase transition of DPPC (Figure S8). The area occupied by the phospholipid molecules in the Petri dish in the experimental system with cyclic stimulation is 76 Å^2 molecule^{-1} corresponding with the area in which phase transition occurs. Linalool and acetic acid induce an increase in Π at the phase transition point. By contrast, triethylamine induces a decrease in Π at the phase transition point. Since linalool is highly hydrophobic, it is assumed that it interacts hydrophobically with the acyl chains of DPPC, which results in an increase in surface pressure. Acetic acid decreases the pH of the aqueous phase. The PO^- in DPPC changes the POH; that is, the hydrophobicity of DPPC increases. As a result, Π of DPPC increases with the addition of acetic acid.[39-41]

Triethylamine, however, is highly water-soluble as a strong base, and the choline moiety of DPPC is deprotonated. The decrease in the hydrophilicity of DPPC may induce more compact packing because of the interaction between the PO^- and choline moieties; as a result, Π decreases with the addition of triethylamine. Thus, γ_e increases and decreases with the addition of triethylamine and linalool, respectively, since $\Pi = \gamma_w - \gamma_e$. ($\gamma_w$ is the surface tension of pure water (~72 mN m^{-1}). The lack of clear discrimination between triethylamine and acetic acid or linalool in 1,2-dioleoyl-*sn*-glycero-3-phosphocholine (DOPC) without phase transition in a Π-*A* isotherm (data not shown) suggests that the amplification of the chemical information of the odor is realized by the physicochemical properties of the molecular layer, that is, phase transition. Consequently, some of the benefits of the dynamic response of the molecular layer to the artificial sniffing system are assured.

Indeed, we examined DOPC instead of DPPC as a phospholipid molecular layer. The results showed that DPPC was still superior to DOPC for odor discrimination under the present conditions (Figure S4). We confirmed that the time-variation of the surface tension is characteristically changed depending on the phospholipid molecular layer, such as DOPC. This suggests that the combination of the different kinds of molecular layers in the present system enhances the discrimination of many kinds of odors in future work.

Additionally, the dynamic response of the sensor was examined using benzene as a nonpolar odorant. The system was not very sensitive to benzene (Figure S5). This suggests that the interaction of the functional group of the odorant molecule with the hydrophilic part of the DPPC is important for identification.

Figures 8 and 9 suggest that the characteristic responses of $\Delta\gamma$ to the three types of odor molecules can be approximately reproduced through numerical calculations based on a simple kinetic model. The figure of eight-shaped rotation in the $\Delta\gamma$ *vs*. flow rate curve for triethylamine in Figure 3c3 is composed of clockwise at the higher flow rate and anticlockwise rotation at the lower flow rate. On the other hand, the rotational direction of $\Delta\gamma$ *vs*. $f(t)$ curves in Figures 8c3 and 9c is anticlockwise. The difference in the direction of rotation may be due to the slight phase difference in the calculation of $\Delta\gamma$ (see Figures S1 and S2) and the distance between location of the platinum plate to measure the surface tension and that of the sensor to measure the flow rate. In addition, a characteristic dynamic response to triethylamine has been reported for another system.[42]

CONCLUSIONS

We demonstrated the characteristic dynamic response of phospholipid molecular layers to different odor molecules in a novel artificial sniffing system. Some of the benefits of the molecular layer to the artificial sniffing system are clarified by the Π-*A* curves, in which the phase transition enhances the chemical information of the odor. The characteristic dynamic response of the monolayers strongly indicates that the DPPC monolayers, which exhibit phase transitions in the Π-*A* curve, are appropriate candidates for use as amplifiers in artificial sniffing. The benefits of the molecular layer were confirmed by numerical calculations based on the rate constants of the adsorption and desorption of the odor onto the molecular layer. The periodic dynamic response of the surface tension reflects the chemical information of the odor.

In this study, we proposed a novel odor-sensing system that mimics "sniffing". A single detector composed of a phospholipid molecular layer could distinguish between several types of odor molecules based on its dynamic response under periodic perturbations. The artificial sniffing developed in this study may provide a novel mechanism for biological sniffing. On the other hand, the frequency of the artificial sniffing, which is lower than that of biological system, suggests the possibility of another mechanism to promote adsorption and desorption of sample gases to membranes. Sensor arraying with analytical methods such as correlation of principal component analysis and prediction with artificial neural networks may be useful to amplify odor distinctions.[27, 28] Although we examined at the shorter period of the flow perturbation, e.g., 5.0 s, it was difficult to identify odors since a sufficient flow rate could not be ensured in the present fan. We should develop the experimental system with a shorter period of flow perturbation to mimic animal sniffing in future work.

Humidity had little effect on the surface tension of the DPPC molecular layer in the actual examinations between 30 and 90%.

This is one of the advantages for gas sensing since semiconductor gas sensors are generally responsive to the humidity.[43]

According to the actual sniffing frequency in some living organisms with a high olfactory frequency,[44] a sensing system with either a short measurement or a higher frequency of sniffing operations is available for the development of practical chemical sensors. As the present system is sensitive to the temperature of the water phase (Figure S6), the influence of the temperature of the water phase should also be considered as an optimization of the experimental conditions for distinguishing odors. On the other hand, linalool used in this study was racemic. Enantioselectivity using the present system should be possible in future work because DPPC is a chiral molecule, and the interaction between chiral molecules may induce a characteristic response in the surface tension depending on the chirality. In addition, it is known that there is a cell-species-dependent bias in the lipid composition of cell membranes in vivo.[45, 46] Therefore, the artificial olfactory system presented here should provide new alternatives to elucidate the olfactory sensing mechanisms of organisms through direct interactions between odor molecules and biological membranes.

ASSOCIATED CONTENT

Supporting Information

The Supporting Information is available free of charge on the ACS Publications website. Additional results for the time variations of γ_{DPPC} and γ for linalool, acetic acid, and triethylamine and the flow rate *vs.* γDPPC or γ curves, time variations of γ for triethylamine and γ *vs*. flow rate curves with different amounts, One cycle of $f(t)$ based on eq. 3, DSC thermograms. (PDF)

AUTHOR INFORMATION

Corresponding Author

E-mail: nakatas@hiroshima-u.ac.jp

Author Contributions

M. Yotsumoto performed the examinations and numerical calculation and wrote the manuscript. M. Matsuo analysed the data and edited the manuscript. H. Kitahata and M. Nagayama developed the numerical model and edited the manuscript. S. Nakanishi and M. Denda discussed the effect of odor molecules and edited the manuscript. S. Nakata developed the experimental system and edited the manuscript. All authors discussed the results and the manuscript.

Notes

The authors declare no competing financial interests.

ACKNOWLEDGMENT

This study was supported by JSPS KAKENHI (grant no. JP20H02712, JP21H00996), Iketani Science and Technology Foundation (0351181-A), the Cooperative Research Program of "Network Joint Research Center for Materials and Devices" (No. 20231004), to S.N., and the JSPS Bilateral Joint Research Project between Japan and the Polish Academy of Sciences. This study was supported by a Sasakawa Scientific Research Grant from the Japan Science Society to M. Y. (2023-6004)

REFERENCES

(1) Mombaerts, P. Genes and Ligands for Odorant, Vomeronasal and Taste Receptors. *Nat. Rev. Neurosci.*, **2004**, *5*, 263-278.
(2) Bushdid, C.; Magnasco, M. O.; Vosshall, L. B.; Keller, A. Humans Can Discriminate More than 1 Trillion Olfactory Stimuli. *Science*, **2014**, *343*, 1370-1372.
(3) Laska, M.; Genzel, D.; Wieser, A. The Number of Functional Olfactory Receptor Genes and the Relative Size of Olfactory Brain Structures Are Poor Predictors of Olfactory Discrimination Performance with Enantiomers. *Chem. Senses*, **2005**, *30*, 171-175.
(4) Lowry, T. W.; Kusi-Appiah, A. E.; Fadool, D. A.; Lenhert, S. Odor Discrimination by Lipid Membranes. *Membranes*, **2023**, *13*, 151.
(5) Denda, M.; Umino, Y.; Kumazawa, N.; Nakata, S. Can Simple Physicochemical Studies Predict the Effects of Molecules on Epidermal Water‐Impermeable Barrier Function? *Exp. Dermatol.*, **2020**, *29*, 393–399.
(6) Tsumoto, K.; Matsuo, H.; Tomita, M.; Yoshimura, T. Efficient Formation of Giant Liposomes through the Gentle Hydration of Phosphatidylcholine Films Doped with Sugar. *Coll. Surf. B*, **2009**, *68*, 98-105.
(7) Vialetto, J.; Rudiuk, S.; Morel, M.; Baigl, D. From Bulk Crystallization of Inorganic Nanoparticles at the Air/Water Interface: Tunable Organization and Intense Structural Colors. *Nanoscale*,**2020**, *12*, 6279-6284.
(8) Fujita, R.: Yotsumoto, M.; Yamaguchi, Y.; Matsuo, M.; Fukuhara, K.; Takahashi, O.; Nakanishi, S.; Denda M. ; Nakata, S. Masking of a Malodorous Substance on 1, 2-Dioleoyl-*sn*-glycero-3-phosphocholine Molecular Layer. *Coll. Surf. A*, **2022**, *634*, 128045-1-7.
(9) Schmidt, R. F. Nociception and Pain. *Fundamentals of Sensory Physiology*, Springer-Verlag, Berlin, DE, **1986**.
(10) Beta C.; Kruse, K. Intracellular Oscillations and Waves. *Annu. Rev. Condens. Matter Phys.*, **2017**, *8*, 239-264.
(11) Getchell, T. V. Functional Properties of Vertebrate Olfactory Receptor Neurons. *Physiol. Rev.*, **1986**, *66*, 772-818.
(12) Verhagen, J. V.; Wesson, D. W.; Netoff, T. I.; White J. A.; Wachowiak, M. Sniffing Controls and Adaptive Filter of Sensory Input to the Olfactory Bulb. *Nat. Neurosci.*, **2007**, *10*, 631-639.
(13) Sobel, N.; Prabhakaran, V.; Desmond, J.E.; Glover, G.H.; Goode, R. L.; Sullivan E.V.; Gabrieli, J. D. Sniffing and Smelling: Separate Subsystems in the Human Olfactory Cortex. *Nature*, **1998**, *392*, 282-286.
(14) Bocca, E.; Antonelli A. R.; Mosciaro O. Mechanical Co-Factors in Olfactory Stimulation. *Acta Otolaryngol*., **1965**, *59*, 243-247.
(15) Frasnelli, J.; Charbonneau, G.; Collignon O.; Lepore, F. Odor Localization and Sniffing. *Chem. Senses*, **2009**, *34*, 139-144.
(16) Porter, J.; Craven, B.; Khan, R. M.; Chang, S. J.; Kang, I.; Judkewitz, B.; Volpe, J.; Settles G.; Sobel, N. Mechanisms of Scent-Tracking in Humans. *Nat. Neurosci.*, **2007**, *10*, 27-29.
(17) Johnson, B. N.; Mainland J. D.; Sobel, N. Rapid Olfactory Processing Implicates Subcortical Control of an Olfactomotor System. *Neurophysiol.*, **2003**, *90*, 1084-1094.
(18) Prescott, J.; James B.; Robert, A. F. Influence of Odor Hedonics, Food-Relatedness, and Motivational State on Human Sniffing. *Chemosens. Percept.*, **2010**, *3*, 85-90.
(19) Nakata, S.; Okunishi, H.; Nakashima, Y. Distinction of Gases with a Semiconductor Sensor Depending on the Scanning Profile of a Cyclic Temperature. *Analyst* **2006**, *131*, 148-154.
(20)Hassan, M. F.; Kamal, E. S.; Michael S. F. Artificial Olfactory Signal Modulation for Detection in Changing Environments. *ACS Sens.*, **2023**, *8*, 527–533.
(21) Nakata S.; Takahara, N. Characteristic Nonlinear Responses of a Semiconductor Gas Sensor to Hydrocarbons and Alcohols under the Combination of Cyclic Temperature and Continuous Flow. *Sens. Actuators B Chem.*, **2020**, *307*, 127635.
(22) Nakata, S.; Akakabe, S.; Nakasuji M.; Yoshikawa, K. Gas Sensing Based on a Nonlinear Response: Discrimination between Hydrocarbons and Quantification of Individual Components in a Gas Mixture. *Anal. Chem.*, **1996**, *68*, 2067-2072.
(23) Misawa, N.; Fujii, S.; Kamiya, K.; Osaki, T.; Takaku, T.; Takahashi, Y.; Takeuchi, S. Construction of a Biohybrid Odorant Sensor Using Biological Olfactory Receptors Embedded into Bilayer Lipid Membrane on a Chip. *ACS Sens.*, **2019**, *4,* 711-716.
(24) Ackels, T.; Erskine, A.; Dasgupta, D.; Marin, A. C.; Warner, T. P.; Tootoonian, S.; Fukunaga, I.; Julia J. H.; Schaefer, A. T. Fast Odour Dynamics Are Encoded in the Olfactory System and Guide Behaviour. *Nature*, **2021**, *593*, 558-563.
(25) Grosmaitre, X.; Santarelli, L. C.; Tan, J.; Luo M.; Ma, M. Dual Functions of Mammalian Olfactory Sensory Neurons as Odor Detectors and Mechanical Sensors. *Nat. Neurosci.*, **2007**, *10*, 348-354.
(26) Arshak, K.; Moore, E.; Lyons, G. M.; Harris J.; Clifford, S. A Review of Gas Sensors Employed in Electronic Nose Applications. *Sens. Rev.*, **2004**, *24*, 181-198.

(27) Jurs, P. C.; Bakken, G. A.; McClelland, H. E., Computational Methods for the Analysis of Chemical Sensor Array Data from Volatile Analytes. *Chemical Reviews*, **2000**, *100*, 2649-2678.
(28) Paulsson, N.; Larsson, E.; Winquist, F., Extraction and Selection of Parameters for Evaluation of Breath Alcohol Measurement with an Electronic Noses, *Sens. Actuator A Phys*., **2000**, *84*, 187-197.
(29) Homma, C.; Tsukiiwa, M.; Noguchi, H.; Tanaka, M.; Okochi, M.; Tomizawa, H.; Hayamizu, Y. Designable Peptides on Graphene Field-Effect Transistors for Selective Detection of Odor Molecules. *Biosens. Bioelectron.,* **2023**, *224*, 115047.
(30) Hierlemann, A.; Gutierrez-Osuna, R. Higher-Order Chemical Sensing. *Chem. Rev.*, **2008**, *108*, 563−613.
(31) Cooper, S. L.; Guan, J., *Advances in polyurethane biomaterials.* Woodhead Publishing, **2016**.
(32) Yan, J.; Guo, X.; Duan, S.; Jia, P.; Wang, L.; Peng, C.; Zhang, S., Electronic Nose Feature Extraction Methods. A review. *Sensors* **2015**, *15*, 27804-27831.
(33) Martins, M. A.; Silva, L. P.; Ferreira, O.; Schröder, B.; Coutinho, J. A.; Pinho, S. P. Terpenes Solubility in Water and Their Environmental Distribution. *J. Mol. Liq.*, **2017**, *241*, 996-1002.
(34) Zaitsau, D. H.; Verevkin S. P.; Sazonova, A. Y. Vapor Pressures and Vaporization Enthalpies of 5-Nonanone, Linalool and 6-Methyl-5-hepten-2-one. Data Evaluation. *Fluid Phase Equilib.*, **2015**, *86*, 140-148.
(35) Mendonça, Â. F.; Pereira S. N.; Lampreia, I. M. Solubility of Triethylamine in Calcium Chloride Aqueous Solutions from 20 to 35°C. *J. Solution Chem.*, **2003**, *32*, 1033-1044.
(36) Dutt, N. V.; Kahol A. P.; Jyothiraju, P. Vapor Pressure of Trimethyl Phosphite and Trimethylamine. *J. Chem. Eng. Data*, **1982**, *27*, 369-370.
(37) Ritter H. L.; Simons J. H. The Molecular State of Acetic Acid Vapor. *J. Am. Chem. Soc.*, **1945**, *67*, 757-762.
(38) Gang M.; Heather, C. A. DPPC Langmuir Monolayer at the Air−Water Interface: Probing the Tail and Head Groups by Vibrational Sum Frequency Generation Spectroscopy. *Langmuir*, **2006**, *22*, 5341-5349.
(39) Liu, H.; Lu, R. Z.; Turcotte J. G.; Notter, R. H. Dynamic Interfacial Properties of Surface-excess Films of Phospholipids and Phosphonolipid Analogs. *J. Colloid Interface Sci*., **1994**, *167*, 378-390.
(40) Caro, A. L.; Niño M. R. R.; Patino, J. M. R. The Effect of pH on Structural, Topographical, and Rheological Characteristics of β-Casein–DPPC Mixed Monolayers Spread at the Air–Water Interface. *Coll. Surf. A*, **2009**, *332*, 180-191.
(41) Kaviratna A. S.; Banerjee, R. The Effect of Acids on Dipalmitoyl Phosphatidylcholine (DPPC) Monolayers and Liposomes. *Coll. Surf. A*, **2009**, *345*, 155-162.
(42) Han, Y.; Liu, Y.; Su, C.; Chen, X.; Zeng, M.; Hu, N.; Su, Y., Zhou. Z, Wei, H.; Yang, Z. Sonochemical Synthesis of Hierarchical WO_3 Flower-like Spheres for Highly Efficient Triethylamine Detection. *Sens. Actuator B Chem*., **2020**, *306*, 127536.
(43) Tai, H.; Wang, S.; Duan, Z.; Jiang, Y. Evolution of Breath Analysis Based on Humidity and Gas Sensors: Potential and Challenges. *Sens. Actuators B*, **2020**, *318*, 128104.
(44) Ackels, T.; Erskine, A.; Dasgupta, D.; Marin, A. C.; Warner, T.; Tootoonian, S.; Fukunaga, I.; Harris, J. J.; Schaefer, A. T., Fast Odour Dynamics Are Encoded in the Olfactory System and Guide Behaviour. *Nature* **2021**, *593*, 558-563.
(45) Daleke, D. L. Regulation of Transbilayer Plasma Membrane Phospholipid Asymmetry. *J. Lipid Res.*, **2003**, *44*, 233-242.
(46) Van Meer, G.; Voelker D. R.; Feigenson, G. W. Membrane Lipids: Where They Are and How They Behave. *Nat. Rev. Mol. Cell Biol.,* **2008**, *9*, 112-124.

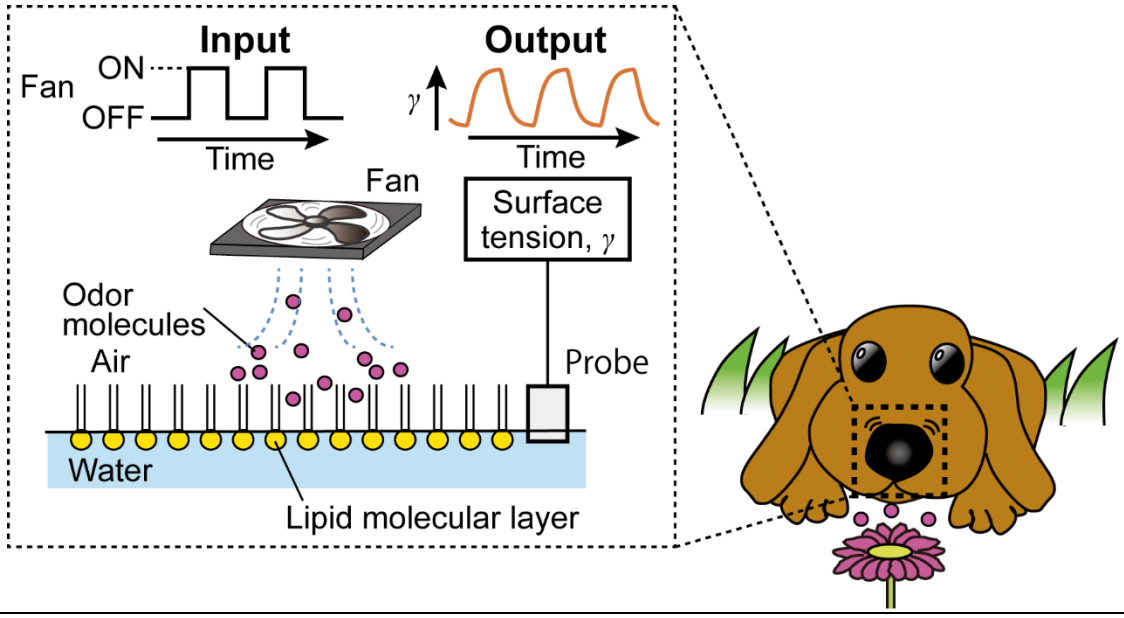
Input
Output
Fan
ON
OFF
Time
γ
Time
Fan
Surface tension, γ
Odor molecules
Air
Probe
Water
Lipid molecular layer

Supporting Information (SI)

Phospholipid molecular layer that enhances distinction of odors based on artificial sniffing

Mai Yotsumoto,[1] Muneyuki Matsuo,[1] Hiroyuki Kitahata,[2] Shinobu Nakanishi,[3] Mitsuhiro Denda,[4] Masaharu Nagayama,[5] Satoshi Nakata[1,*]

1. Graduate School of Integrated Sciences for Life, Hiroshima University, 1-3-1 Kagamiyama, Higashi-Hiroshima, Hiroshima 739-8526, Japan

2. Graduate School of Science, Chiba University, Yayoi-cho 1-33, Inage-ku, Chiba 263-8522, Japan

3. Shiseido Global Innovation Center, 1-2-11, Takashima-cho, Nishi-ku, Yokohama, Kanagawa 220-0011, Japan

4. Institute for Advanced Study of Mathematical Sciences, 8F High-Rise Wing, Nakano Campus, Meiji University, 4-21-1 Nakano, Nakano-ku, Tokyo, 164-8525, Japan

5. Research Institute for Electronic Science, Hokkaido University, N10 W8, Kita-Ward, Sapporo 060-0810, Japan

1. Time variation of γ_{DPPC} and γ for linalool, acetic acid, and triethylamine, and the flow rate *vs.* γ_{DPPC} or γ curve

Time-variations of γ_{DPPC} and γ for linalool, acetic acid, and triethylamine and the flow rate *vs.* γ_{DPPC} or γ curves are shown in Figure S1. When the fan voltage was switched on, γ_{DPPC} without odors was decreased rapidly, and then increased a steady value slowly (see b1 in Figure S1). When the fan voltage was switched off, γ_{DPPC} was increased rapidly, and then slowly decreased a steady value. The average value of γ_{DPPC} was ~ 60 mN m^{-1}, and the peak-to-peak amplitude of γ_{DPPC} under the periodic perturbation was 0.4 mN m^{-1}.

The dynamic surface tension was characteristically changed with the addition of different odors. As for the stimulation of linalool, the baseline of γ_{DPPC} was decreased, but the amplitude of oscillation was increased (peak-to-peak amplitude: 0.8 mN m^{-1}) (see b2 in Figure S1). When the fan voltage was switched on, γ_{DPPC} was decreased. When the fan voltage was switched off, γ_{DPPC} was increased rapidly and then gradually. As for the stimulation of acetic acid, the amplitude was slightly increased, but the waveform of surface tension was changed. When the fan voltage was switched on and off, γ_{DPPC} was decreased and increased rapidly, respectively, and then reached a constant value. As for the stimulation of triethylamine, the response of the surface tension was inverted. That is, γ_{DPPC} was increased and decreased, respectively when the fan voltage was switched on and off.

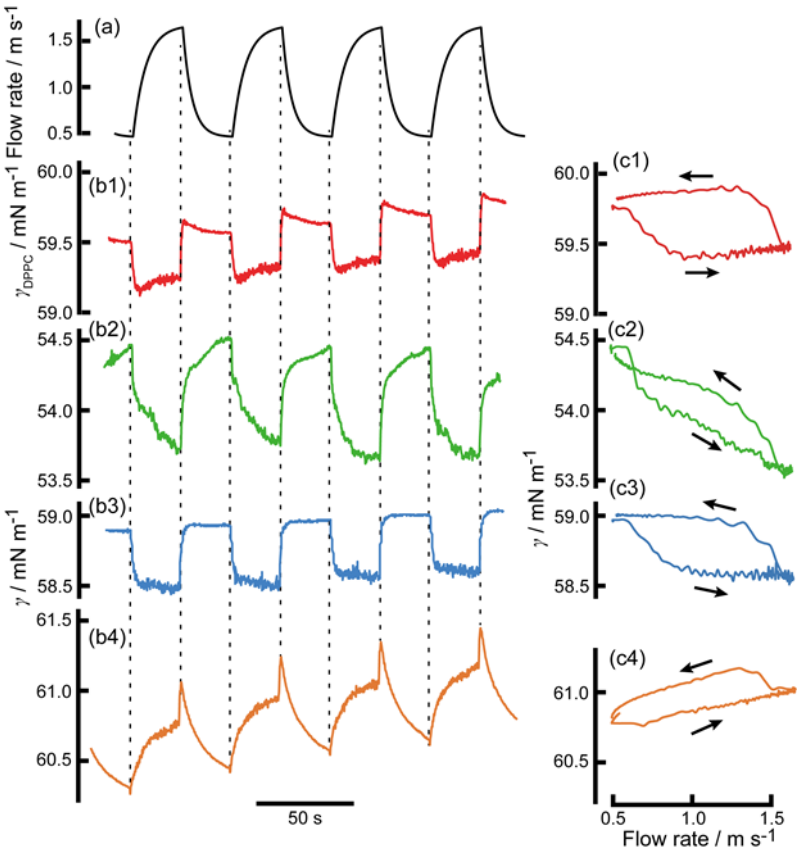

Figure S1. Time variation of (a) the flow rate and (b) the surface tension for the DPPC molecular layer distributed on the water surface under the application of periodic blowing air (1) without odors (γ_{DPPC}) and (2-4) with odors (γ). (c) One cycle of the flow rate *vs.* γ_{DPPC} or γ curve for (b). The measured odors were (2) linalool, (3) acetic acid, and (4) triethylamine. The individual amount of odors soaked into a filter paper was 1.55 mmol. The data correspond to those for Figure 3.

2. Time variation of γ_{DPPC} and γ for trimethylamine, and the flow rate *vs.* γ_{DPPC} or γ curve at the different concentrations

The dynamic surface tension changed characteristically with the concentration of triethylamine. As the concentration of triethylamine increased, the amplitude of the oscillations increased and the positive slope of flow rate *vs.* γ curve increased.

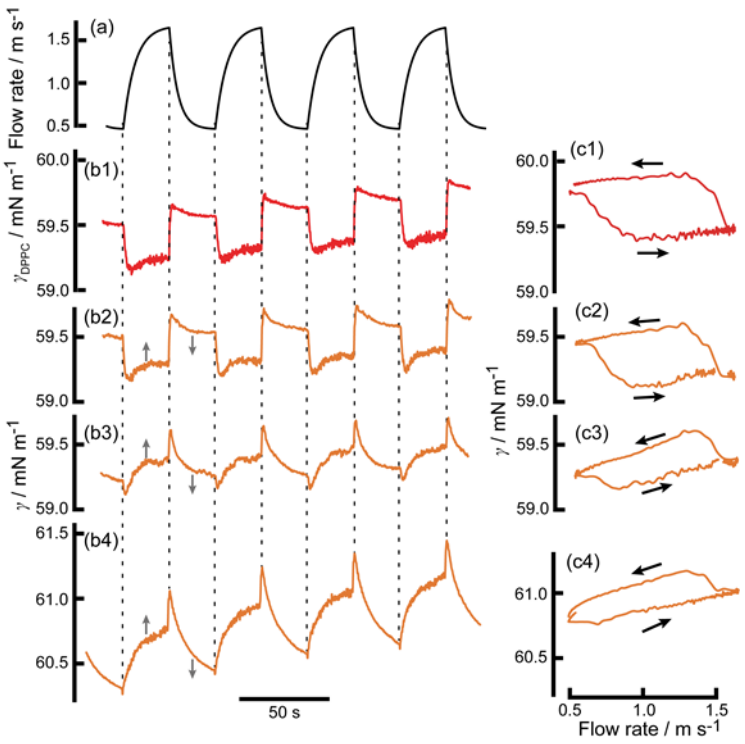

Figure S2. Time variation of (a) the flow rate and (b) the surface tension for the DPPC molecular layer distributed on the water surface under the application of periodic blowing air (1) without odors (γ_{DPPC}) and (2-4) with triethylamine (γ). (c) One cycle of the flow rate *vs.* γ_{DPPC} or γ curve for (b). The amounts of triethylamine were (2) 0.31, (3) 0.78, and (4) 1.55 mmol. The data correspond to those for Figure 4.

3. Time variation of γ_{DPPC} and γ for linalool, acetic acid, and triethylamine, and the flow rate *vs.* γ_{DPPC} or γ curve at the lower density of DPPC on water

The time variation of the surface tension was measured at the lower density of DPPC on water, i.e., A = 100 Å^2 molecule^{-1}, as shown in Figure S3. The dynamic response was changed

depending on A. That is, the experimental condition of A is an important factor to distinguish odors in the present system.

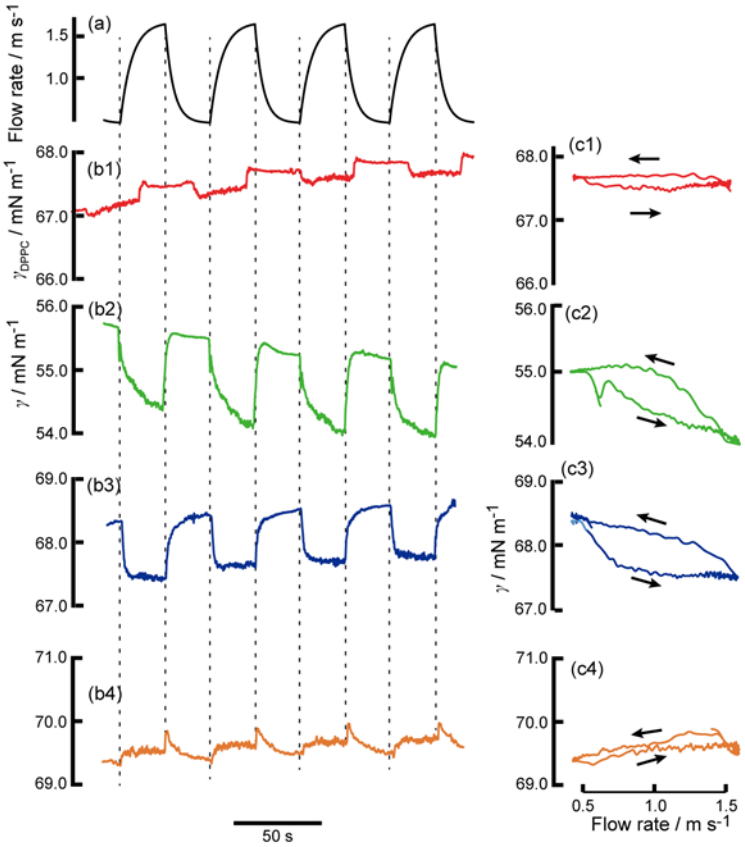

Figure S3. Time variation of (a) the flow rate and (b) the surface tension for the DPPC molecular layer distributed on the water surface under the application of periodic blowing air (1) without odors (γ_{DPPC}) and (2-4) with odors (γ). (c) One cycle of the flow rate *vs.* γ_{DPPC} or γ curve for (b). The measured odors were (2) linalool, (3) acetic acid, and (4) triethylamine. The individual amount of odors soaked into a filter paper was 1.55 mmol.

4. Time variation of the surface tension for the DOPC molecular layer with the addition of the odors

Time variations of γ_{DOPC} and γ for linalool, acetic acid, and triethylamine are shown in Figure S4. The dynamic responses of γ for DOPC were different from those for DPC except for linalool.

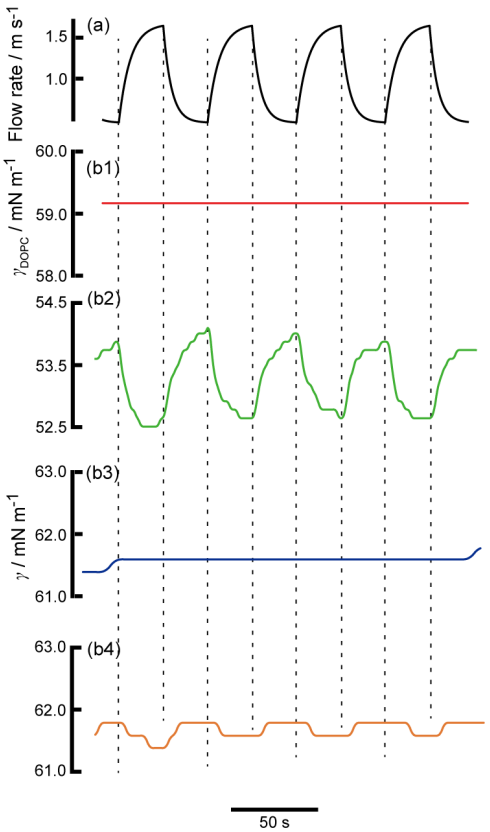

Figure S4. Time variation of (a) the flow rate and (b) the surface tension for the DOPC molecular layer distributed on the water surface under the application of periodic blowing air (1) without odors (γ_{DOPC}) and (2-4) with odors (γ). The measured odors were (2) linalool, (3) acetic acid, and (4) triethylamine. The individual amount of odors soaked into a filter paper was 1.55 mmol.

5. Time variation of γ and the flow rate *vs.* γ curve for benzene as a nonpolar odor

Time-variation of γ and the flow rate *vs.* γ curve for benzene as a nonpolar odor molecule are shown in Figure S4. The dynamic response of γ was not changed very much with the addition of benzene. This result suggests that nonpolar odor molecules are not sensitive to the DPPC molecular layer.

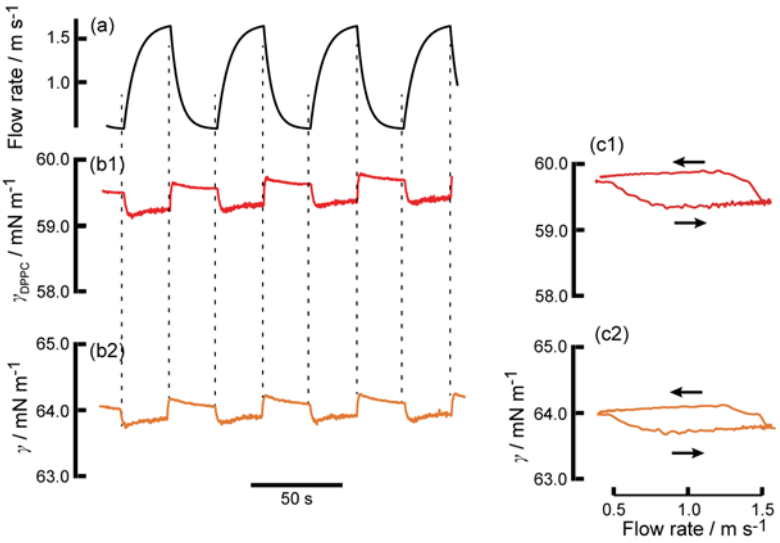

Figure S5. Time variation of (a) the flow rate and (b) the surface tension for the DPPC molecular layer distributed on the water surface under the application of periodic blowing air (1) without odors (γ_{DPPC}) and (2) with benzene (γ). (c) One cycle of the flow rate *vs.* γ_{DPPC} or γ curve for (b). The individual amount of odors soaked into a filter paper was 1.55 mmol.

6. Time variation of γ_{DPPC} and the flow rate *vs.* γ_{DPPC} curve for air without odor at different temperature

In order to clarify the effect of the temperature on the present system, time-variation of γ_{DPPC} was measured at different temperature, as indicated in Figure S5. The time-variation of γ_{DPPC} was changed depending on the temperature.

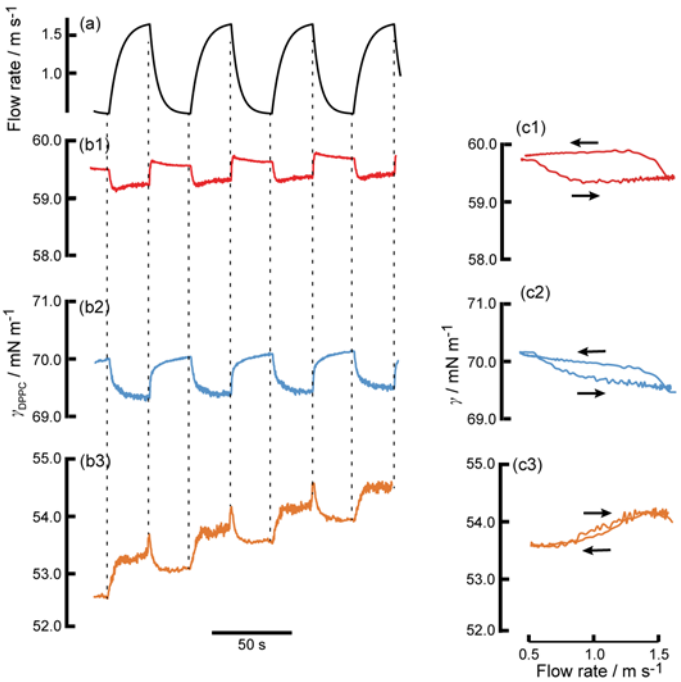

Figure S6. Time variation of (a) the flow rate and (b) the surface tension for the DPPC molecular layer distributed on the water surface under the application of periodic blowing air without odors (γ_{DPPC}). (c) One cycle of the flow rate *vs.* γ_{DPPC} curve for (b). Temperature of the water phase were (1) 25, (2) 10, and (3) 40℃.

7. Numerical calculation of the artificial sniffing

To understand dynamic responses to odor molecules under the application of periodic flow, we performed numerical calculation based on eqn1-4. Figure S6 shows one cycle of $f(t)$ used in the numerical calculation based on eqn 3.

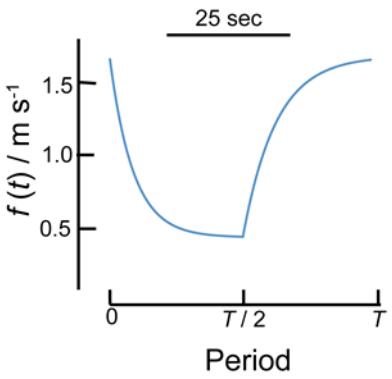

Figure S7. One cycle of $f(t)$ based on eqn 3.

8. DSC thermograms of DPPC or the mixture of DPPC and triethylamine

Thermograms of DPPC were measured using a Differential Scanning Calorimeter (DSC) thermometer (DSC4000, PerkinElmer, MA) at a scanning rate of 3 K min^{-1}. Powder of DPPC (1.2×10^{-6} mol) as the dried sample was put in an aluminum vessel, and 7 μL of water or 1.2 mol/L triethylamine aqueous solution was added to the sample (M_{DPPC} : $M_{triethylamine}$=1 : 1).

DSC was measured to thermodynamically evaluate the effect of triethylamine on DPPC. Figure S7 shows DSC thermograms for DPPC or the mixture of DPPC and triethylamine at the range of -20 ~ 60℃. The temperature of the phase transitions for DPPC were observed around 41 and 35℃ with the addition of H_2O. Here, we defined T_{p-I} and T_{p-II} as the temperatures of the thermogram peaks at the higher and lower temperature range,

respectively. Both of T_{p-I} and T_{p-II} were decreased by the addition of triethylamine. Thus, the addition of triethylamine affects the phase transition of DPPC.

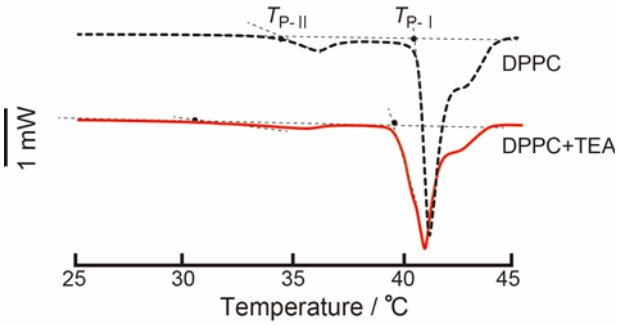

Figure S8. DSC thermograms (heating scan) for DPPC as a wet sample (black line) and for DPPC-triethylamine mixtures (red line).